

# Towards an Image-based Indicator for PAD Classification and Localization

Christina Gillmann\*, John M. Matsuura<sup>†</sup>, Hans Hagen\* and Thomas Wischgoll<sup>†</sup>

\*Computer Graphics and HCI Group, University of Kaiserslautern, Kaiserslautern, Germany  
E-mail: c\_gillma@cs.uni-kl.de, hagen@cs.uni-kl.de

<sup>†</sup>Advanced Visual Data Analysis, Wright State University, Dayton, USA  
E-mail: john.matsuura@wright.edu, thomas.wischgoll@wright.edu

**Abstract**—Peripheral Artery Disease (PAD) is an often occurring problem caused by narrowed veins. With this type of disease, mostly the legs receive an insufficient supply of blood to sustain their functions. This can result in an amputation of extremities or strokes. In order to quantify the risks, doctors consult a classification table which is based on the pain response of a patient. This classification is subjective and does not indicate the exact origin of the PAD symptoms. Resulting from this, complications can occur unprompted. We present the first results for an image-based indicator assisting medical doctors in estimating the stage of PAD and its location. Therefore, a segmentation tree is utilized to compare the changes in a healthy versus diseased leg. We provide a highlighting mechanism that allows users to review the location of changes in selected structures. To show the effectiveness of the presented approach, we demonstrate a localization of the PAD and show how the presented technique can be utilized for a novel image-based indicator of PAD stages.

**Index Terms**—Medical Visualization, Image Segmentation, Visual Analytics

## I. INTRODUCTION

Peripheral Artery Disease (PAD) is a disease caused by narrowed veins [22]. Resulting from this, mostly the legs are not supplied with enough blood to properly maintain their functions. PAD is an increasing problem in modern society triggered by factors such as obesity, smoking, and lack of exercise [16]. Patients affected by PAD experience pain to a degree such that they are no longer able to walk further distances. In extreme cases, open sores cannot heal properly, extremities need to be amputated as the tissue of a patient starts to become necrotic, or strokes can occur.

Patients that are affected by PAD can be classified to different categories, considering the Fontaine Scale [20] or the Rutherford Scale [2]. These reach from minor pain symptoms (stage 1) to necrotic tissue (stage 4). Although these scales can provide a first classification of the PAD stage of a patient, they are based on the subjective sense of pain graded by the patient. Especially for stages 2 and 3, the diagnose can be rather vague and the progression of the disease is hard to estimate.

The need for an objective measure of PAD stages was initially mentioned by Mohler et al. [15]. In their work, they proposed that a visual PAD measure as *an unmet clinical need in the evaluation of patients with PAD who are candidates for regeneration therapy with stem cells or other angiogenic therapies*. This means that the slice-by-slice reviewing methodology in clinical daily routine lacks the ability to visually indicate the progression and location of PAD. Based on this, it is hard for clinicians to determine a proper treatment or to predict the progress of PAD for a specific patient.

To solve this problem, this paper presents a CT-scan based measure to compare a healthy leg of a patient with its unhealthy leg affected by PAD. We accomplish this by utilizing a hierarchical and fuzzy image segmentation approach leading to a separation of a patient's legs, and further separate the patient's bone, veins, muscles, and soft tissue. Based on this, we define ratios expressing the vitality of a leg to achieve a quantitative measure. These measures are encoded by an intuitive visualization to allow further analysis by the medical expert. In order to allow medical users to spatially locate the biggest influence of PAD in human legs, we support an interactive exploration of PAD measures by highlighting voxel values with a significant difference between healthy and diseased leg.

Therefore, this work contributes:

- Requirements for an objective PAD measurement
- A basis for an image-based indicator for PAD classifications
- Intuitive analysis for spatial and structural PAD localization

We show the effectiveness of the presented approach by applying it to real world datasets of patients that are affected by PAD. We show that the presented system can help to locate PAD and form hypothesis for creating a novel objective image based PAD measure.

## II. RELATED WORK

PAD classifications are currently achieved by reviewing specific patient histories [4], [7] before considering an image-based diagnosis. Although this enhances the probability to

detect patients with PAD diseases, medical images are required to confirm this hypothesis.

Matthew and Kramer [21] summarized, the current state of the art in imaging methods that can be utilized to diagnose PAD disease. Their work shows that many PAD patient are not detected. This work aims to increase the accuracy of imaging techniques in order to achieve a better and faster treatment for patients.

Tang et al. [17] mentioned the advantages of CT-scans during PAD diagnosis. They suggest further investigation of CT-scan image processing techniques. This work picks up this notion and utilizes a segmentation approach to allow an objective comparison and identification of PAD in CT scans.

CPR (Curved Planar Reformation) relates to the flattening of a vessel along its centerline by sampling the vessel cross-sections [5]. The quality of the resulting planar gray-scale images are highly dependent on the chosen sampling strategies. In addition, the visualization of several vessels raise the question of their arrangement in a plane [13], [14], [19]. In contrast to planar visualization approaches volume rendering can be used to create a three-dimensional visualization of the monitored heart. The main problem for this class of visualization is the applied transfer function. Especially in medical datasets, they can be hard to find. Several approaches use additional knowledge obtained from cardiovascular modeling or simulations to create suitable and more accurate transfer functions [6], [12], [18]. Although these methods have been shown to be successful in displaying vessels and their calcification, these methods are not able compare a healthy and a diseased leg properly. In contrast to this, the presented approach provides a visual comparison of both legs of a patient and enables the clinician to locate the PAD disease more accurate.

Methods utilizing multi-modal visualization [23] or MRI based flow measures [27] are aiming to identify and quantify the occlusion in an affected vein. Although this is a good starting point, it is not sufficient for comparing the diseased and healthy leg of a patient. Therefore, the presented method utilizes a segmentation approach to allow a direct comparison of both legs.

In order to identify the changes in image data, a variety of image comparison metrics is available as shown in [8], [24], [28], including distance-based functions. These usually require an initial image registration step in order to generate suitable results [29]. Contrary to this, the presented method works without a registration step and is based on a segmentation approach to allow the comparison of arbitrarily located and shifted legs. Spyridonos et al. [25] presented a technique to compare medical images and identify their differences based on the Hausdorff distance. Although the technique is able to compare different images, the images need to be very similar to produce suitable results. In clinical daily routine, the acquired images can be very diverse even though they show the same aspect. To solve this problem, the presented work utilizes a segmentation that is suitable for all input scenarios in images and compares the resulting segments.

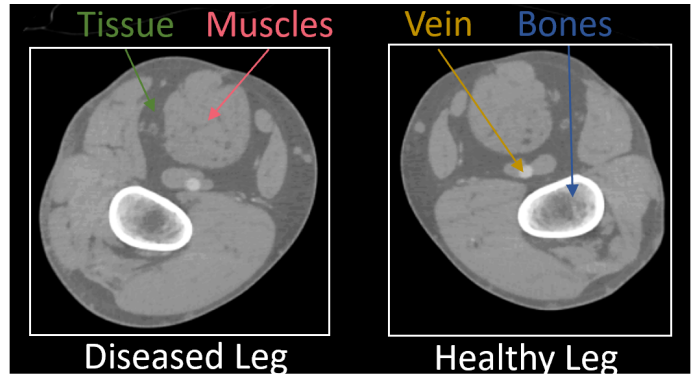


Fig. 1: Slice of an a CT scan of a PAD patient with both legs present. The different structures that are visible are highlighted. Here, differences between both legs are hard to determine.

Geurts et al. [9] presented a technique to compare segmentation results based on statistical shape models. Although this is a good starting point for the presented work, we are refining this technique by examining the structural behavior of different segment and highlight the identified changes.

### III. APPLICATION AND REQUIREMENTS ANALYSIS

PAD is a disease that results from an accumulation of plaque on vascular walls in the extremities of patients. It can cause wounds that do not heal properly, strokes, and can require amputation of the affected extremity when tissue starts to become necrotic. Many PAD patients are diagnosed very late or sometimes not at all which can cause dangerous complications. The state of the art analysis shows that there is a clear lack of a diagnosis method which allows a reliable and quantitative diagnosis of PAD.

This is due to slice-by-slice reviewing technique utilized in clinical daily routine. With this technique, medical doctors scroll through the stack of images that are contained in a CT scan, while solely looking at one slice at a time. Doctors are trained to create a three-dimensional image in their head. Here, it can be hard to determine the difference between a healthy and a diseased leg, as shown in Figure 1. In addition, it is hard to determine, if specific substructures vary depending on the considered leg.

To solve this problem, we initially achieved a list of requirements that need to be fulfilled by a visual indicator of PAD. We achieved this list through long discussions with our medical collaborators and a careful literature review. The list can be found above.

**R1:** *Quantitative comparison of diseased and healthy structures of extremities.* In order to understand the effect of PAD to a patient, it is not sufficient to solely examine the veins of a patient. Vessels can be slightly blocked along the walls, not leading to a visible blockade. Still, this can effect surrounding muscle tissue, which needs to be detected.

**R2: Localization of PAD.** In order to determine a proper treatment for a patient or plan a surgery, clinicians need to know, where to intervene exactly.

**R3: Intuitive Exploration of patient data.** [10] PAD diseases can be very unspecific and its effects differ from patient to patient. This requires an intuitive exploration of patient data, where doctors can observe aspects, they are interested in.

**R4: Inclusion of uncertainty information.** Medical image data is usually affected by uncertainty, which means that image pixels can vary in their intensity. This information needs to be included and visualized in any computational step to show the certainty of the computed results to the clinician.

#### IV. METHODS

In order to achieve an objective visual indicator for the progression of a PDA that fulfills the formulated requirements, we present a visual workflow especially designed for medical doctors, as shown in Figure 2. Starting from the input image, we utilize a fuzzy and hierarchical segmentation approach to compare the sizes of specific substructures in a healthy and diseased leg of a patient. In addition, we provide a back mapping, where all voxels in a structure are selected that exceed a user defined threshold. Based on this information, we are able to present intuitive visualizations for clinicians that highlight the structures with the biggest differences.

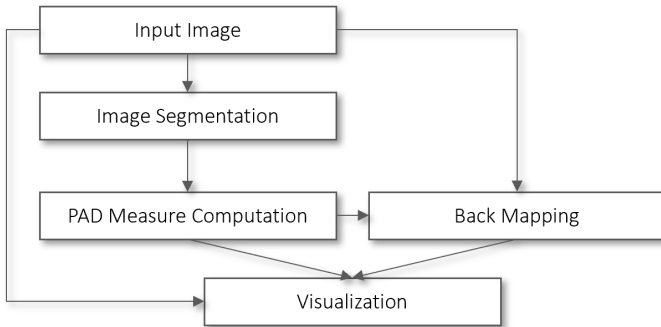


Fig. 2: Workflow of the presented Method. Starting from the input image, a segmentation approach is applied to compute PAD specific measurements. Users can select voxels in the diseased leg that differ drastically from the healthy leg. This back mapping, the PAD measure charts and the original image form the resulting visualization.

The input of the presented workflow is a CT scan, which is defined as a three-dimensional image that is referred to as  $I$  in the following. For the input image  $I$ , we are able to access each voxel  $x$  by  $I(x)$ . This function outputs a value  $s$ , which is the intensity value of the input image in the voxel  $x$ .

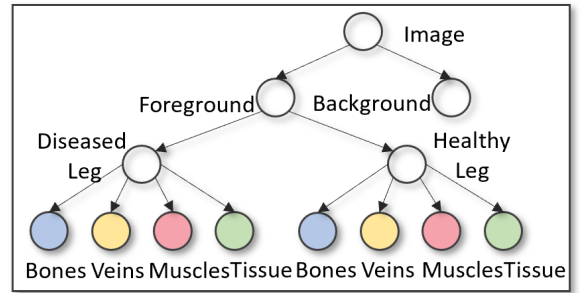
##### A. Segmentation

In order to compare a diseased and a healthy leg of a patient and to identify the differences, a separation of the input image into the individual structures encoded therein is required.

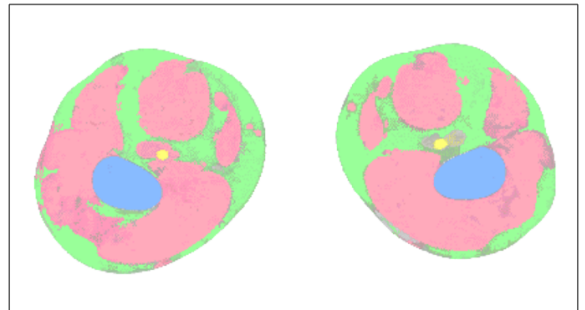
When comparing the legs of a patient on a CT scan, the provided comparison technique needs to aware of areas of

the legs that are captured, different positions of the legs and knee prosthesis. Here, it can be hard to determine an overall approach that is suitable for each case.

This can be achieved by a segmentation algorithm. The segmentation approach applied here is described by Gillmann et al. [11] and defines a hierarchical and fuzzy image segmentation approach designed for medical applications. This approach is chosen because we are interested in a hierarchical composition of the structures encoded within the image, starting with a separation of the legs of a patient and continuing with re-segmenting each segment into its different structures, such as muscles and tissue. The fuzzy approach helps to obtain a description of each structure that is more precise compared to other methods and able to counteract sources of errors commonly occurring in CT scans, such as the partial volume [3] effect or reconstruction artifacts [26] that can lead to an unstable segmentation result. The work of Gillmann et al. showed evidence in having a high precision and being suitable for arbitrary medical image data.



(a) Segmentation tree  $T$ .



(b) Segmentation result for the example presented in Figure 1.

Fig. 3: Segmentation tree structure and resulting segmentation. a) Segmentation tree structure capturing both legs and their substructures. b) Segmentation result utilizing the defined segmentation tree structure. Areas, where the segmentation algorithm was not able to output certain results are shown transparent.

As a result of the hierarchical and fuzzy segmentation approach, we are able to obtain a segmentation tree that separates the CT scan of a patients legs hierarchically as shown in Figure 3. Here, the input image is initially separated into foreground and background. The foreground can be further

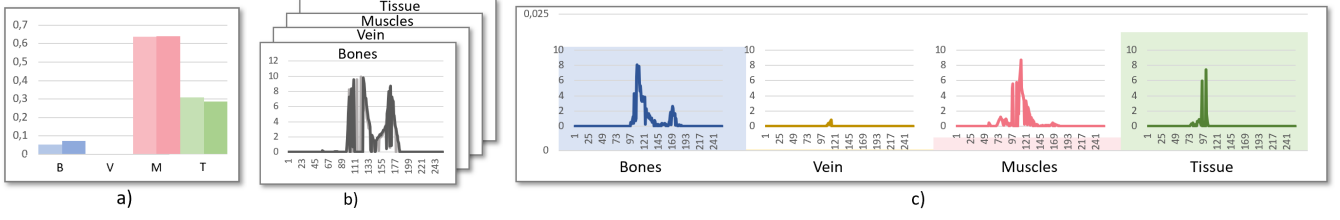


Fig. 4: PAD Measures. a) Volume ratios of bone, veins, muscles and tissue in the healthy and diseased leg. b) Weighted histogram of the healthy and diseased leg segment. c) Combined visualization including the difference of volume ratios and the difference of weighted histograms.

separated into diseased leg and healthy leg. Each of the legs can be further separated into bones (blue), vein (yellow), muscles (red) and soft tissue (green). This scheme is utilized for all datasets that are subject of analysis.

For each of the mentioned segments ( $i$ ), the segmentation algorithm generates an image which includes the same number of pixels as the input image. Instead of the input intensity value of the CT scan, each pixels holds a probability that describes the likelihood of that pixel to belong to the selected segment of the segmentation tree, referred to as  $\omega_i$ . For each node  $i$  in the segmentation tree  $T$ , this weight is referred to as  $\omega_i$ . In addition to the weight, each node additionally holds a reference to its parent, which is defined as  $p(i)$ .

The effectiveness of the selected segmentation approach can be reviewed in Figure 3 b). Here, the designed segmentation tree was applied to the example dataset from Figure 1. Both legs were successfully separated from the background. Furthermore, all structures in each leg are captured correctly. When the algorithm was not able to make a clear decision to which structure a pixel belongs to, the pixel is shown with less opacity.

Although the utilized segmentation algorithm is especially designed for medical users, our approach is able to use any hierarchical and fuzzy image segmentation approach. A review of hierarchical image segmentation approaches can be found in [1].

## B. PAD Measures

When reviewing the CT scan presented in Figure 3 a), it becomes clear that the classic slice-by-slice reviewing method utilized in clinical daily routine is not able to indicate the difference between a healthy and a diseased leg of a patient. Therefore, the presented method aims to visualize the differences in the captured images utilizing the presented segmentation tree. Here the goal is to allow medical doctors to classify the stage of PAD and spatially localize it.

In order to achieve this, we utilize two different measures to compare the physical appearance of structures in the legs of a patient. The first measure, the **volume ratio**, describes the percentage of a leg that is occupied by a specific structure, such as muscles. The second measure, the **weighted histogram**, presents a histogram of all present weights in a depicted structure of the patient's legs.

To compute the **volume ratio** of a leaf node in the presented segmentation tree, we require a function  $v$  that is able to compute the volume of an arbitrary node in  $T$ . Therefore all weights of a segment need to be summed up to obtain the volume of the represented structure. To obtain the **volume ratio** that defines the percentage occupancy of a structure in a leg, we need to divide the volume of the leaf node  $i$  by the volume of its parent  $p(i)$ . More formally, the **volume ratio**  $v_r(i, p(i))$  is computed by:

$$v_r(i, p(i)) = \frac{\sum_{x \in I} \omega_i(x)}{\sum_{x \in I} \omega_{p(i)}(x)} \quad (1)$$

Figure 4 a) shows the results for **volume ratios** of bones, veins, muscles and tissues in the left and right leg. As it can be observed, it is hard to compare the relative volume for each of the structures of the two legs. To solve this problem, we computed the absolute difference between the diseased and healthy leg for each structure to be able to identify the degree of change for each structure, as Figure 4 c) indicates. This allows a quick identification of the structures with sizes affected the most by PAD.

Although this is a good starting point to localize the effect of PAD, this does not show how exactly the structure changes. This is a crucial information for clinicians, as they are trying to adjust a patient's treatment based on this measure.

To solve this problem, we also utilize a weighted histogram for each of the observed structures. In comparison to a classic histogram, where the number of voxels holding a specific intensity value are counted and separated into bins, this segmentation approach is able to refine the histogram computation. Instead of increasing the value of a histogram, when a specific intensity occurs, we are adding the weight of the respective node to the histogram. Therefore, we can define a **weighted histogram** for each segmentation node in the tree  $T$ . The **weighted histogram**  $h_\omega(v)$  as:

$$h_\omega(v) = \sum_x \omega_i(x) I_{(x)=v} \quad (2)$$

This means that a voxel is counted strongly if it strongly belongs to the respective node in the segmentation tree and weakly if it does not belong strongly to the respective segmentation node. This allows a histogram computation that

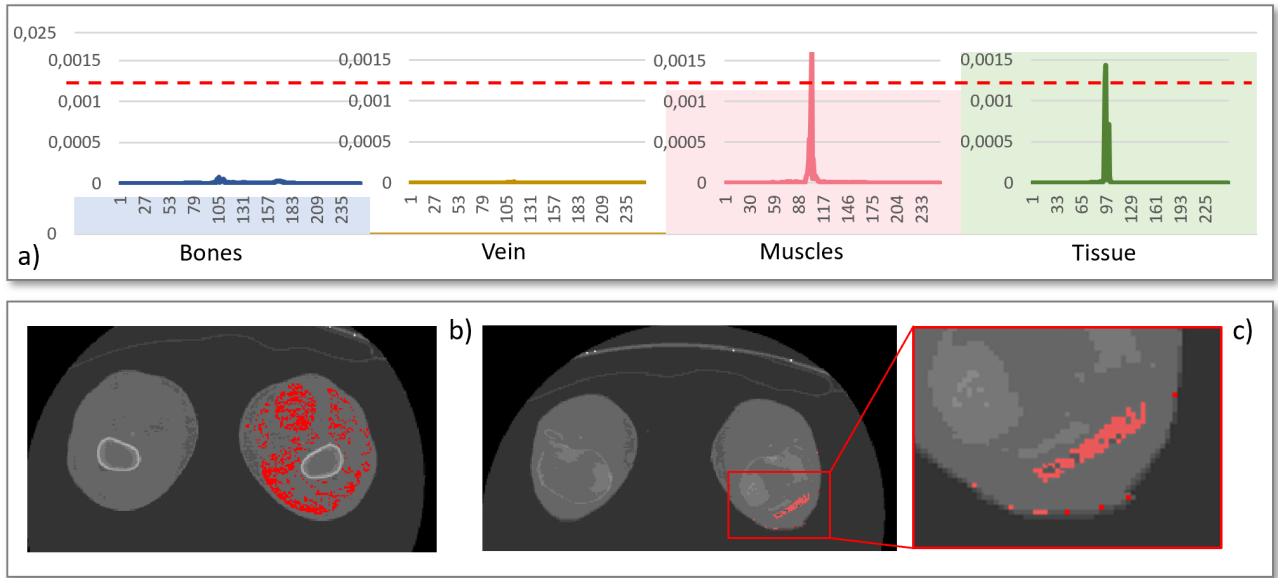


Fig. 5: General examination of PAD effects and their distribution in the diseased leg. a) PAD Measures visualization. User can set a threshold that selects voxels in the diseased leg with a high difference to the healthy leg. b) Highlighted voxels in the muscle of the patient. c) Highlighted voxels in the tissue of the patient with a closeup.

summarized the occurrences of intensity values respectively to their segmentation result.

An example for the **weighted histogram** computation of the muscles in the diseased and healthy leg can be found in Figure 4 b). As it can be seen, it is hard to compare the difference between the two histograms. To solve this problem, the absolute difference between the histograms is computed, as shown in Figure 4 c). This allows users to identify the intensity values whose occurrence is varying mostly in a depicted structure.

In order to present the results for the differences of **volume ratios** and the difference of **weighted histograms** for bones, veins, muscles and tissue to medical doctors, the computed measures are combined to an overall visualization, as shown in Figure 4 c). The visualization is separated into four parts, one for each structure. We are utilizing a consistent color scheme to differentiate between the structures, as shown in Figure 3. The background of each image shows the difference of **volume ratios** of each structure as bar charts. Here, users can directly identify structures that differentiate in the legs mostly. In addition, each part of the visualization holds the difference of **weighted histograms** as the foreground. The histograms are shown with the same scale such that users can directly compare all structures and identify peaks in the graphs.

The presented visualization allows users to obtain an impression of how the volumes of two structures differ within the shown structures. In addition, it allows to identify the structure of the leg with the highest difference and also to see the exact intensity values in each structure that causes the difference.

### C. Back Mapping

Although the presented PAD measures can provide a good impression about the stage of a PAD, it does not provide a spatial localization of areas in the the human leg that are affected the most. To solve this problem, the presented workflow allows highlighting of image voxels that hold an intensity value differing in the healthy and the diseased leg. This is accomplished by letting the user select a threshold that needs to be exceeded. In the presented PAD measures plot, users can define the substructure they are interested in and the threshold, as shown in Figure 5 (red line).

The highlighting is embedded in the slice-by-slice reviewing procedure that is utilized in clinical daily routine. This allows an easy to understand representation for medical users.

Here, all voxels that exceed the user defined threshold  $t$  in the respective difference of histograms of a selected structure  $i$ . More formally, this means we are creating a new image, where:

$$I^*(x)_i = \begin{cases} c * \omega(x) , & \text{if } h_\omega(I(x)) > t \\ I(x) , & \text{else} \end{cases} \quad (3)$$

where  $c$  is a selected highlight color by the user. For all values that are not exceeding the defined threshold  $t$ , the voxel intensity values from the original image is shown. Contrary to this, if an intensity value exceeds the user defined threshold, all voxels with the respective intensity value in the original image are highlighted by the user defined color  $c$ .

The  $\alpha$  value of all voxels that are highlighted is adjusted according to the respective value  $\omega_i(x)$  of the selected segmentation node. If the weight of the current voxel is 0, the highlight color will be transparent. This means that the highlighted voxel

is not a part of the selected segment and not of interest in the current investigation. Contrary to this, if the weight of a voxel in the selected node is 1, the voxel is shown opaque and in the selected highlight color, as shown in Figure 5 b) and c).

This allows medical doctors to review the CT scan in the slice-by-slice visualization approach and identify regions that are highly affected by PAD. As users can select the structure where they want to have a highlighting, they can directly relate the effect of PAD to the different structures of the human body.

## V. RESULTS

To show the effectiveness of this work, we utilized the presented workflow to examine real world datasets of patients facing a PAD disease. The data was retrieved from Premier Health’s Miami Valley Hospital in Dayton (Ohio). The shown patients gave permission to use their datasets, which are anonymized. Each dataset was labeled by a medical doctor with the PAD scale as currently utilized in clinical daily routine. The presented cases show stage 2 and stage 3 PAD, which are the one that clinicians are most interested in.

### A. PAD Localization

The first scenario we investigated is a general PAD localization and distribution analysis in the diseased leg of a patient shown in Figure 1. For the analysis, the entire dataset was utilized. Here, the patient was initially classified with PAD stage 2, which is an early stage of the PAD progression. In the presented case, medical doctors are interested in identifying the effect of PAD to the different structures in the human leg.

As mentioned before, each leg is separated into its bones, veins, muscle and tissue. Figure 5 a) shows the resulting PAD measure visualization presented in this work. When reviewing the plot, it can be observed that the difference in the volume ratios is very low in the bones and vein. This indicates that the PAD did not lead to significant size changes in the respective structures. Contrary to this, differences are high when considering the muscles and tissue of the patient. This impression is strengthened, when reviewing the differences of weighted histograms for both structures. Here, we selected a threshold covering both peaks of the shown histograms to investigate the areas in the human body that is affected the most by the PAD disease.

As Figure 5 b) shows, the effects of PAD are widely distributed throughout the entire muscle tissue. The highlighted voxels can be found in almost all slices, when scrolling through the entire volume. This indicates that the first effects of PAD is a change in the muscle tissue throughout the entire diseased leg.

Contrary to this, Figure 5 c) shows a cluster of voxels that is highlighted in the tissue around the knee cap of the patient. Interestingly, almost no voxels are highlighted in the remaining slices. PAD patients usually experience pain when walking and the detected cluster around the kneecap can be a reason for this pain. This helps medical doctors to adjust the utilized therapy and focus on the condition of a patient’s knee.

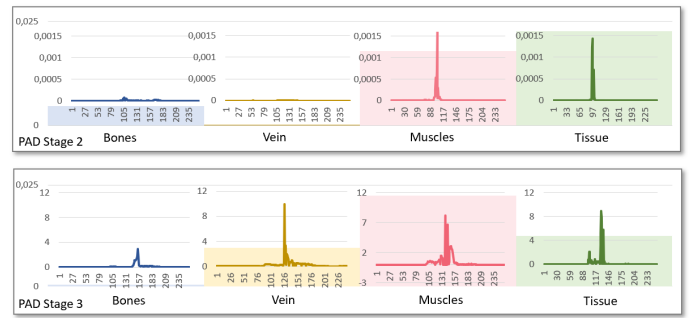


Fig. 6: Hypothesis forming for an image-based indicator of PAD stages. Top: PAD plot for a patient classified with stage 2. Down: PAD plot for a patient classified with stage 3.

### B. Hypothesis Forming

The second scenario we investigated with the presented technique is the case of a hypothesis forming for an image-based measure to classify the PAD progress of a patient.

In the presented case, we compared the presented PAD plots obtained from a stage 2 and a stage 3 PAD patient. As mentioned before, the current scales utilized in clinical daily routine are based on a patient-specific pain response that is hard to classify. With the presented method, we want to equip medical doctors with an objective tool that allows them to create objective measures for PAD scale classification.

The results of the made comparison can be reviewed in Figure 6. The top PAD plot presents the obtained measure for a PAD patient that is currently classified as stage 2. The down PAD plot shows the results for a PAD patient in stage 3.

Although the number of tested subject is not sufficient to provide statistical evidence, the presented method can be used to provide an initial hypothesis forming. When reviewing both test subjects, the first hypothesis is that the bones of a patient are not affected significantly by PAD, regardless of the current stage. Furthermore, the overall difference in the volume ratios calculated for the vein of a patient increases when considering a further stage. In addition, the vein’s morphology seems so change as well during stage 3. The same hypothesis arises when considering the plots for the muscles of the two patients. Interestingly, the difference in the volume ratios of the patient facing a stage 3 PAD decreases, when considering the tissues of the patient. Here, the hypothesis arises that the tissue is not an visual indicator to classify the PAD stages.

The identified hypothesis are subject for further investigation throughout a clinical study that aims to provide statistical evidence for these findings. The results indicate that an image-based measure for PAD stages is not a one-dimensional scale, as multiple structures are contributing to the PAD diseases stage. This hypothesis is strengthened by the feedback of our medical collaborators, which claim:

*Our initial approach was to look specifically at acute limb ischemia to determine whether we can identify differences in the tissues that could predict a potentially salvageable limb from one that cannot be saved. Current decisions regarding*

amputation are based on physical examination or measurement of compartment pressures. With better refinement of this approach we hope this approach might also play a greater role in chronic limb ischemia.

The presented visualization clearly shows the advantage of the presented PAD plots. Regardless of patient position in the CT-scan device, the area that is captured within the CT-scan device or legs that contain prosthesis, the utilized segmentation approach can capture each leg and its substructures and thus they can be compared.

## VI. DISCUSSION

The following section aims to discuss the defined requirements for an objective PAD measure as shown in Section III.

**R1:** The presented methodology provides measures to compare a healthy and a diseased extremity of a patient objectively. Here, different structures in the legs can be compared as well considering their histograms and their volume. The comparison works independently from the position of the patient and the location of the legs in the considered CT scan as long as they are present with a similar volume. In cases where patients have an implanted artificial knee cap or other metal surgery supplies in their extremities, the affected areas can not be considered for the computation of the PAD measures. Metal massively affects the resulting CT scan and would therefore corrupt the PAD measure computation.

**R2:** The localization of PAD is achieved by the back mapping procedure presented in this work. Users can select structures and set a threshold that allows to select the voxels which are highlighted. Here, users can examine the effects of PAD to different structures in the patient's extremities.

**R3:** The intuitive exploration of patient data is a crucial point in promoting a novel visualization technique. Our medical collaborators agreed that the data representation is easy to understand and the interaction works intuitive. They also appreciated the inclusion of the state of the art slice-by-slice reviewing procedure in the presented approach.

**R4:** The inclusion of uncertainty information is a key point of the presented approach. The utilized segmentation approach outputs a fuzzy segmentation allowing to express areas that cannot be separated clearly. This information is utilized to refine the volume computation for each structure in the patients extremities as well as the histogram computations. In addition, the back mapping is color coded according to the uncertainty of the segmentation result. This leads to an overall objective PAD measure that includes uncertainty information throughout each computational step.

## VII. CONCLUSION

This work is an initial step towards an image-based indicator for PAD classification and localization. We achieved this by utilizing a hierarchical and fuzzy segmentation approach. This allows to isolate the different structures in each leg of a patient and compare these structures. The comparison is achieved by an intuitive visualization. In order to identify the effects of the PAD to different structures in the leg, we allow a visual

highlighting in the state of the art slice-by-slice reviewing technique utilized in clinical daily routine.

## ACKNOWLEDGMENT

We would like to thank the Premier Health Hospitals in Dayton (Ohio) for permission to work with the anonymized patient data shown in this work.

## REFERENCES

- [1] P. Arbelaez, M. Maire, C. Fowlkes, and J. Malik. Contour detection and hierarchical image segmentation. *IEEE Trans. Pattern Anal. Mach. Intell.*, 33(5):898–916, 2011.
- [2] H. AT, C. MH, T.-J. D, and et al. Peripheral arterial disease detection, awareness, and treatment in primary care. *JAMA*, 286(11):1317–1324, 2001.
- [3] J. F. Barrett and N. Keat. Artifacts in ct: Recognition and avoidance. *RadioGraphics*, 24(6):1679–1691, 2004.
- [4] S. Bellmunt, M. Roqu, D. Osorio, H. Pardo, J.-R. Escudero, and X. Bonfill. Healthcare quality indicators of peripheral artery disease based on systematic reviews. *European Journal of Vascular and Endovascular Surgery*, 48(1):60 – 69, 2014.
- [5] G.-P. Bonneau, T. Ertl, and G. M. Nielson, editors. *Scientific Visualization: The Visual Extraction of Knowledge from Data*. Springer, 1 edition, 2006.
- [6] C. Correa and K.-L. Ma. Size-based Transfer Functions: A New Volume Exploration Technique. volume 14, pages 1380–1387, 2008.
- [7] D. Dhanoa, M. O. Baerlocher, A. J. Benko, J. F. Benenati, M. D. Kuo, S. R. Dariushnia, S. Faintuch, M. Midia, and B. Nikolic. Position statement on noninvasive imaging of peripheral arterial disease by the society of interventional radiology and the canadian interventional radiology association. *Journal of vascular and interventional radiology : JVIR*, 27 7:947–51, 2016.
- [8] V. D. Ges and V. Starovoitov. Distance-based functions for image comparison. *Pattern Recognition Letters*, 20(2):207 – 214, 1999.
- [9] A. Geurts, G. Sakas, A. Kuijper, M. Becker, and T. v. Landesberger. Visual comparison of 3d medical image segmentation algorithms based on statistical shape models. In V. G. Duffy, editor, *Digital Human Modeling. Applications in Health, Safety, Ergonomics and Risk Management: Ergonomics and Health*, pages 336–344. Springer International Publishing, 2015.
- [10] C. Gillmann, H. Leitte, T. Wischgoll, and H. Hagen. From Theory to Usage: Requirements for successful Visualizations in Applications. In *IEEE Visualization Conference (VIS) - C4PGV Workshop*, 2016.
- [11] C. Gillmann, R. G. Maack, T. Post, T. Wischgoll, and H. Hagen. An uncertainty-aware workflow for keyhole surgery planning using hierarchical image semantics. *Visual Informatics*, 2(1):26 – 36, 2018. Proceedings of PacificVAST 2018.
- [12] C. Gillmann and P. Salz. Improving Visual Communication for EIT-Based Lung Research. In *Pacific Visualization Symposium (PacificVis), 2014 IEEE*, volume 10, pages 291–295, 2014.
- [13] C. Gillmann, T. Wischgoll, and H. Hagen. Visual Exploration in Surgery Monitoring for Coronary Vessels. In *IEEE Visualization Conference (VIS) - VIP Workshop*, 2015.
- [14] A. Kanitsar, R. Wegenkitti, D. Fleischmann, and M. E. Gröller. Advanced Curved Planar Reformation: Flattening of Vascular Structures. In *IEEE Transactions on Visualization and Computer Graphics*, volume 1, pages 99–108, 2012.
- [15] C. Kramer, M. Yadava, and J. Lindner. Chapter 7 - imaging for regenerative therapy for {PAD}. In E. R. Mohler and B. H. Annex, editors, *Regenerative Medicine for Peripheral Artery Disease*, pages 95 – 116. Academic Press, Boston, 2016.
- [16] I. J. Kullo and T. W. Rooke. Peripheral artery disease. *New England Journal of Medicine*, 374(9):861–871, 2016.
- [17] G. L. Tang, J. Chin, and M. R. Kibbe. Advances in diagnostic imaging for peripheral arterial disease. 8:1447–55, 10 2010.
- [18] G. Lăthén, S. Lindholm, R. Lenz, and M. Borga. Automatic Tuning of Spatially Varying Transfer Functions for Blood Vessel Visualization. In *IEEE TVCG (SciVis Proceedings)*, volume 18, pages 2345–2354, 2012.
- [19] N. Lee and M. Rasch. Tangential Curved Planar Reformation for topological and orientation invariant Visualization of Vascular Trees. In *EMBS Annual International Conference*, volume 28, 2006.

- [20] T. Loosemore, T. Chalmers, and J. Dormandy. A meta-analysis of randomized placebo control trials in Fontaine stages III and IV peripheral occlusive arterial disease. *International angiology : a journal of the International Union of Angiology*, 13(2):133-142, June 1994.
- [21] R. C. Mathew and C. M. Kramer. Recent advances in magnetic resonance imaging for peripheral artery disease. *Vascular medicine*, 23(2):143-152, 2018.
- [22] K. Ouriel. Peripheral arterial disease. *The Lancet*, 358(9289):1257 - 1264, 2001.
- [23] A. W. Pollak, P. T. Norton, and C. M. Kramer. Multimodality imaging of lower extremity peripheral arterial disease. *Circulation: Cardiovascular Imaging*, 5(6):797-807, 2012.
- [24] R. J. Radke, S. Andra, O. Al-Kofahi, and B. Roysam. Image change detection algorithms: A systematic survey. *Trans. Img. Proc.*, 14(3):294-307, Mar. 2005.
- [25] P. Spyridonos, G. Gaitanis, I. D. Bassukas, and M. Tzaphlidou. Gray hausdorff distance measure for medical image comparison in dermatology: Evaluation of treatment effectiveness by image similarity. *Skin research and technology : official journal of International Society for Bioengineering and the Skin (ISBS) [and] International Society for Digital Imaging of Skin (ISDIS) [and] International Society for Skin Imaging*, 19(1):498-506, 2013.
- [26] N. Strumas, O. Antonyshyn, M. Yaffe, G. Mawdsley, and P. Cooper. Computed tomography artefacts: An experimental investigation of causative factors. *Canadian Journal of Plastic Surgery*, 6(1):23-29, 1998.
- [27] B. Versluis, P. J. Nelemans, R. Brans, J. E. Wildberger, G.-W. H. Schurink, T. Leiner, and W. H. Backes. Functional MRI in peripheral arterial disease: Arterial peak flow versus ankle-brachial index. In *PLoS one*, 2014.
- [28] Z. Wang, A. C. Bovik, H. R. Sheikh, and E. P. Simoncelli. Image quality assessment: From error visibility to structural similarity. *Trans. Img. Proc.*, 13(4):600-612, Apr. 2004.
- [29] B. Zitov and J. Flusser. Image registration methods: a survey. *Image and Vision Computing*, 21(11):977 - 1000, 2003.